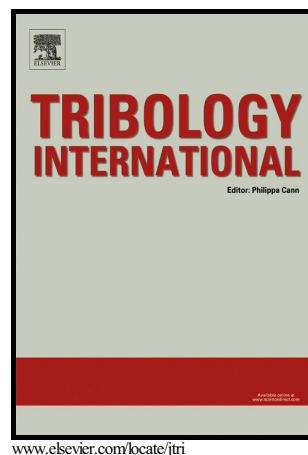# Author's Accepted Manuscript

Friction, wear and tribofilm formation with a [NTf2] anion-based ionic liquid as neat lubricant

A. Hernández Battez, D. Blanco, A. Fernández-González, M.T. Mallada, R. González, J.L. Viesca

TRIBOLOGY INTERNATIONAL

Editor: Philippa Cann

www.elsevier.com/locate/jtri

Cite this article as: A. Hernández Battez, D. Blanco, A. Fernández-González, M.T. Mallada, R. González and J.L. Viesca, Friction, wear and tribofilm formation with a [NTf2] anion-based ionic liquid as neat lubricant, *Tribiology International,* http://dx.doi.org/10.1016/j.triboint.2016.06.038

Friction, wear and tribofilm formation with a [NTf$_2$] anion-based ionic liquid as neat lubricant

A. Hernández Battez[a,d*], D. Blanco[a], A. Fernández-González[b], M.T. Mallada[c], R. González[c,d], J.L. Viesca[a,d]

[a]Department of Construction and Manufacturing Engineering, University of Oviedo, Asturias, Spain
[b]Department of Physical and Analytical Chemistry, University of Oviedo, Asturias, Spain
[c]Department of Marine Science and Technology, University of Oviedo, Asturias, Spain
[d]Department of Design and Engineering, Bournemouth University, Poole, BH12 5BB, UK

[*]Corresponding author: aehernandez@uniovi.es

Abstract

This paper presents the tribological behavior of methyltrioctylammonium bis(trifluoromethylsulfonyl)imide [N$_{1888}$][NTf$_2$] ionic liquid as neat lubricant in a steel-steel contact. A ball-on-disk reciprocating rig was used: firstly, at constant frequency (15 Hz) under both variable loads (40 to 120 N) and sliding distances (216, 324 and 432 m); and secondly, at different frequencies (10 to 30 Hz) and constant both load (80 N) and sliding distance (432 m). Slight friction variations and increasing wear with rising loads was found at constant frequency. Different behavior was found at constant load. The tribofilm thickness formed on the worn surface was closely related to testing conditions and controlled tribological behavior.

Keywords: ionic liquid; friction; wear; tribofilm thickness.

1. Introduction

Among the technical innovations contributing to sustainable development, lubrication science plays a significant environmental role, especially in energy saving and CO$_2$ emissions reduction by increasing the fuel efficiency and extending the service life of machines [1]. Since lubrication is focused on reducing friction, minimizing wear, evacuating heat, removing contaminants and improving efficiency, it is very important the development of novel advances in lubrication of industrial applications such as: internal combustion engines, turbines, hydraulic systems, compressors, transmissions, industrial vehicles, bearings, metal forming, etc. [2]. In general, different approaches can be taken in order to reduce friction in mechanical systems from the lubrication point of view. Firstly, the use of low friction coatings has had great advances in the last 20-30 years as dry lubrication technology. Secondly, the use of textured surfaces has been an interesting approach, achieving friction reduction by about 25% [3]. Thirdly, the utilization of low viscosity oils turns in another solution for decreasing the energy losses from viscous work, but this solution implies the use of new and better additive packages. Finally, the use of ionic liquids in lubrication, as neat lubricant or additive, has become in an active research line since 2001 [4].

Ionic liquids (ILs) are salts composed of ions that melt below the normal boiling point of water. Their growing interest is related to their physicochemical properties which can be tuned by varying the

constituent ions [5]. They exhibit a number of unique features: high thermal stability, large liquid range, non-flammability, negligible vapor pressure, high viscosity, which represent potential advantages over many other lubricants [6]. The first reported use of ionic liquids as lubricant occurred in 1961, when fluorine molten salts were used in tests at high temperature bearings [7]. In 2001, similar molten salts were evaluated for the first time as synthetic lubricants fluids [4] and from that time, these substances have received increasing attention as novel lubricant fluids [8-11].

Many research works about the application of ionic liquids as neat lubricant have exhibited their remarkable potential for this purpose [12-20]. Imidazolium-based ionic liquids with [PF_6] and [BF_4] anions were widely used [21-26] but despite of their good tribological performance, the hydrolysis products of those anions are highly corrosive and toxic [27]. This fact provoked the study of new [FAP] [12, 28-36] and [NTf_2] anion-based ILs [37-46]. The great lubricating performance of these more stable fluorine anions is directly related to their capacity to form protective metal fluoride tribofilms, especially at high load conditions [11]. Typically, the inorganic anion is likely to react with any exposed metal surface, since compounds related to the anion are usually found on the wear scar during surface characterization [12, 19, 47]. On the other hand, this kind of reaction suggests that, since the compound is already in an ionic form, the anion could interact easier with the surface than other traditional substance in lubrication like the ZDDP, which has to be broken down before the interaction occurs [48].
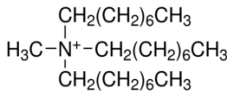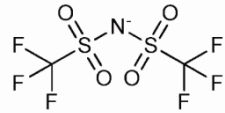
In order to complement the knowledge about [NTf_2] anion-based ionic liquids as neat lubricants, this work explores for the first time the tribological performance of the methyltrioctylammonium bis(trifluoromethylsulfonyl)imide ([N_{1888}][NTf_2]) ionic liquid applied to a steel-steel contact under variable test conditions in order to assess the feasibility of its tribological use in the way that it is commercially available.

2. Experimental details

2.1 Ionic liquid

The ionic liquid methyltrioctylammonium bis(trifluoromethylsulfonyl)imide ([N_{1888}][NTf_2]), commercially available from Io-Li-Tec (Ionic Liquid Technologies GmbH), was used as pure lubricant in this work. Main properties and description of this ionic liquid are shown in Table 1.

Table 1. Ionic liquid properties.

IUPAC NAME (CAS NUMBER)	Purity (%)	Density 20ºC (g/cm^3)	Mol. Weight	Viscosity 40ºC (cP)
Methyltrioctylammonium bis(trifluoromethylsulfonyl)imide (375395-33-8)	99	1.105 [49]	648.85	200.7 [49]

Chemical structure

Cation	Anion
$C_{25}H_{54}N^+$	$C_2F_6S_2O_4N^-$

$[N_{1888}]$ $[NTf_2]$

2.2. Tribological tests

A Bruker UMT-3 tribometer using a ball-on-disk configuration with reciprocating motion was used in this research. Two different types of tribological tests were made in order to study friction, wear and tribofilm formation in a steel-steel contact. In a first stage, the testing conditions were: 15 Hz of frequency, load values of 40, 60, 80, 100 and 120 N (corresponding to maximum contact pressures of 1.67, 1.91, 2.1, 2.26 and 2.41 GPa, respectively) and duration of 30, 45 and 60 minutes (corresponding with sliding distances of 216, 324 and 432 m, respectively). In a second stage, tribological tests were made under a fixed load and sliding distance of 80 N and 432 m, respectively, using frequency values of 10, 15, 20, 25 and 30 Hz. Both types of tribological tests were conducted under a stroke length of 4 mm.

All these assays were made at room temperature and 20–30% of relative humidity. 25 μL of ionic liquid was used in each test assuring a fully-flooded condition to obtain the friction coefficient. Friction coefficient was recorded during the tests and wear volume was measured on the disk's surface using confocal microscopy (Leica DCM 3D). Finally, each test condition was repeated at least three times.

The upper (balls) and lower (disks) specimens used are both manufactured from AISI 52100 steel. The chemical composition and physical description of both specimens are shown in Table 2. Balls and disks were cleaned with heptane in an ultrasonic bath during 5 minutes before tribological tests and also before worn surface characterization. After cleaning in heptane the specimens were rinsed in ethanol and then air dried.

Table 2. Description of the specimens used in tribological tests.

	Chemical composition (%)					
	C	Si	Mn	Cr	P	S
AISI 52100	0.98–1.1	0.15–0.30	0.25–0.45	1.30–1.60	0.025	0.025
	Dimensions		Hardness		Roughness (Ra)	
Chrome steel balls	9.5 mm diameter		63 HRC		0.01 μm	
Steel disks	10 mm diameter × 3 mm thick		190-210 HV_{30}		0.02 μm	

2.4. Surface characterization

Scanning electron microscopy (SEM), energy dispersive spectroscopy (EDS) and X-Ray photoelectron spectroscopy (XPS) were also employed to analyze and evaluate the interaction of the ionic liquids with the worn surface for tests conducted at 45 and 60 minutes under loads of 40, 80 and 120 N. Since XPS results suggested that the tribolayer grows with test duration, samples tested at 30 minutes were not considered for surface analysis as the tribolayer was expected to be too thin for the analysis technique proposed. SEM-EDS analysis was made using an acceleration voltage of 20 kV. In addition, XPS measurements were carried out with a SPECS photoelectron spectrometer equipped with a Phoibos 100 MCD analyzer and a monochromatized X-ray Al source (1486.7 eV). Pressure in the analysis chamber was kept below $5·10^{-9}$ mbar throughout all the experiments. Depth-profiling was performed with an argon ion gun working at 10 mA and 3000 eV with an estimated etching ratio for steel of 1.2 Å·s^{-1}. C1s band of spurious carbon was used to compensate charge shift when necessary. Mathematical analysis of the bands and curve fitting was carried out using CasaXPS software. 70% Gaussian – 30% Lorentzian product curves and Shirley type baselines were used for curve fitting unless otherwise stated.

3. Results and discussion

3.1. Tribological tests at constant frequency (15 Hz).

Fig. 1 shows both the average friction coefficient and wear volumes measured in all tests under five loads (40, 60, 80, 100 and 120 N) and three sliding distances (216, 324 and 432 m). The results are given with the standard deviation (error bars), which did not reach 10% in any case. From a friction coefficient point of view, results exhibited a similar behavior (measured COF values around 0.04) regardless of load and sliding distance except for the high wear value of the test with both lowest load and testing time, maybe

because of the tribochemical reaction that form tribolayer is more efficient at higher loads and depend on testing time [25]. On the contrary, it can be seen the expected growth of wear volume with increasing load, showing slight differences for each load among all sliding distances tested. However, the wear values increased with sliding distance under the highest load (120 N) probably because the rate of destruction of the protective tribofilm formed at high load and temperature was quicker than its rate of formation [42].
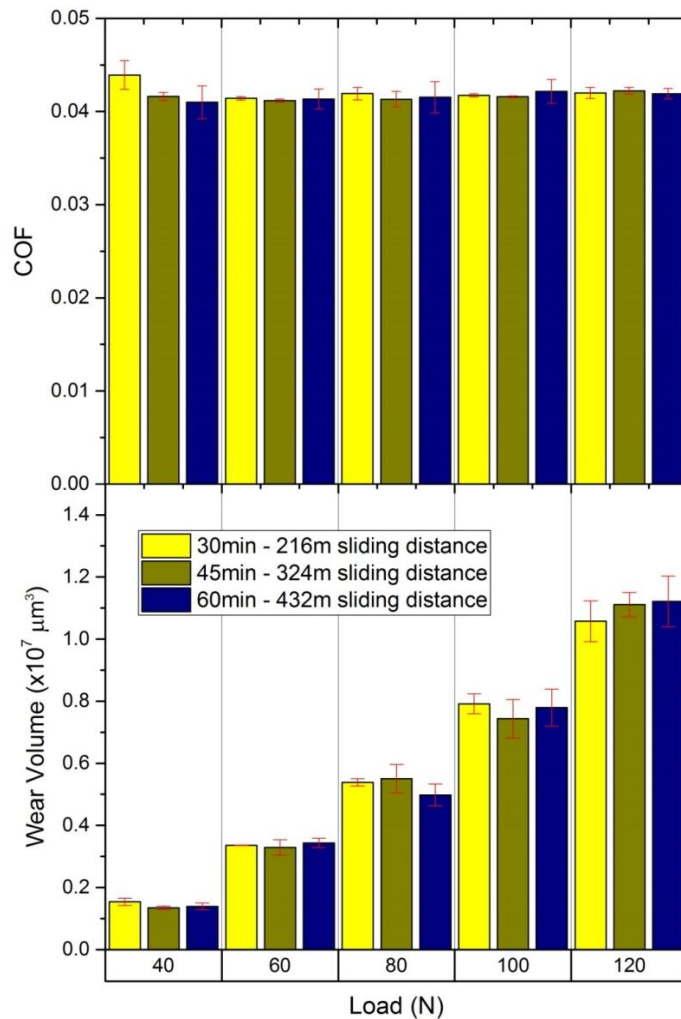

Fig. 1. Tribological results from tests made at 15 Hz.

Fig. 2 shows SEM images of the wear scar obtained in the tests under three loads (40, 80 and 120 N) and two test durations (45 and 60 min). These images display the whole wear track width on the disks and wear mechanisms can be explained from this observation. The wear track width rises as expected with increasing load and the slight differences between tests made at 45 and 60 minutes for the same load are in agreement with wear volume measurements previously shown in Fig. 1. Plastic deformation was found

on the edge of the wear scar on all samples regardless of both load and sliding distance. In addition, tests performed at the lowest load showed a smoother appearance than that corresponding to higher loads. Finally, the EDS analysis was also carried out to further study the worn surface. However, this analysis only showed the elements present in the specimens maybe because of the penetration of this technique is in the micron range and the tribofilm formed by the IL-surface chemical interaction is usually in the nano range. Taking into account this fact, XPS analysis was needed to complement the information provided by the EDS analysis.
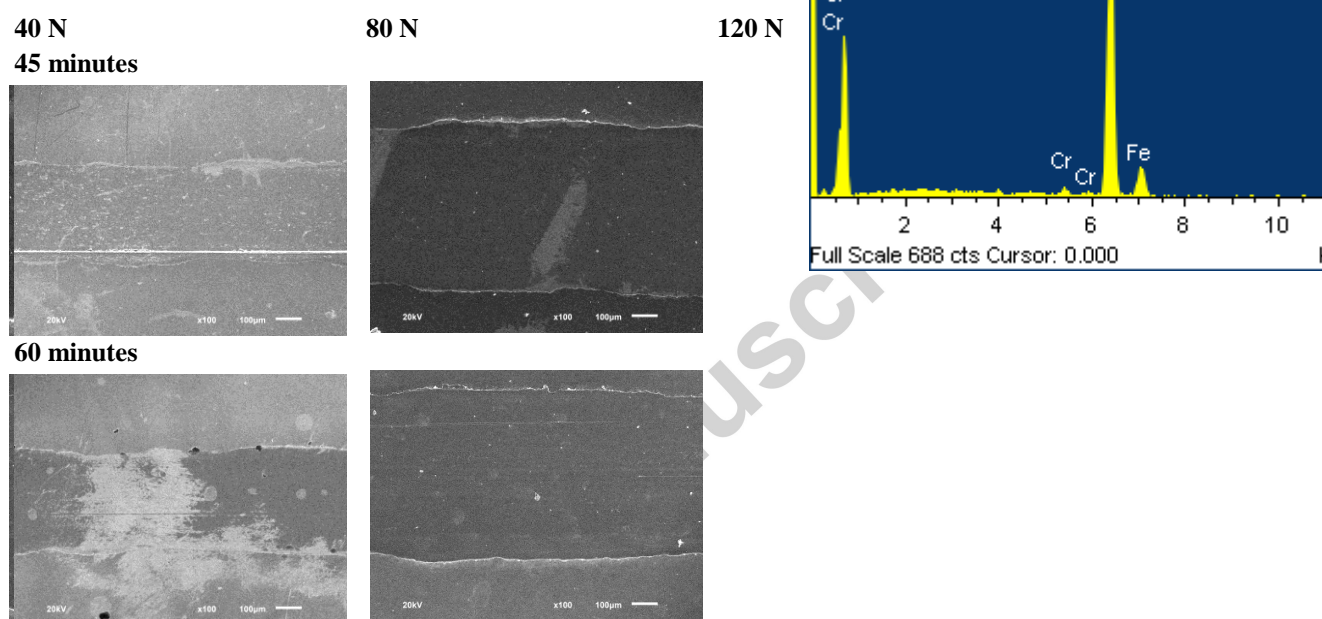

Fig. 2. SEM images (magnification: x100, scale length: 100 μm) from the wear surface after tribological tests made at 15 Hz.

A high resolution XPS analysis of the surface regarding Fe, O, F, N and S was performed in the wear scar of samples assayed for 45 and 60 minutes. As shown in Fig. 3, Fe is clearly present in three different overlapping bands at near 708, 711 and 713 eV. The lowest binding energy (E_B) could be congruent with metallic iron and the second with iron oxides [50], whereas the highest E_B seems to be related to iron with an important withdrawal of electron density, like iron fluorides or sulphides [51]. However, although the behaviour of this band is somehow consistent with the behaviour of F1s band (both bands decrease with depth), there are several evidences which difficult this assignation: i) the band is detected in every sample even in those samples (or depths) where no F or S could be detected; ii) when present, F1s band appears close to 689 eV which does not agree with the position for iron fluorides (~685.0 eV [35]) but does agree with fluorine in [NTf$_2$] anion [52-53]. From a semi-quantitative point of view, the Fe$_2$O$_3$ / Fe ratio is

between 2 and 2.7 for samples assayed at 120 or 80 N, respectively. This ratio drastically grows to 5.2 in tests conducted with the lowest load (40 N). Since iron oxide is present in the surface, the higher the load the higher the damage produced, removing bigger amounts of iron oxide from the surface.
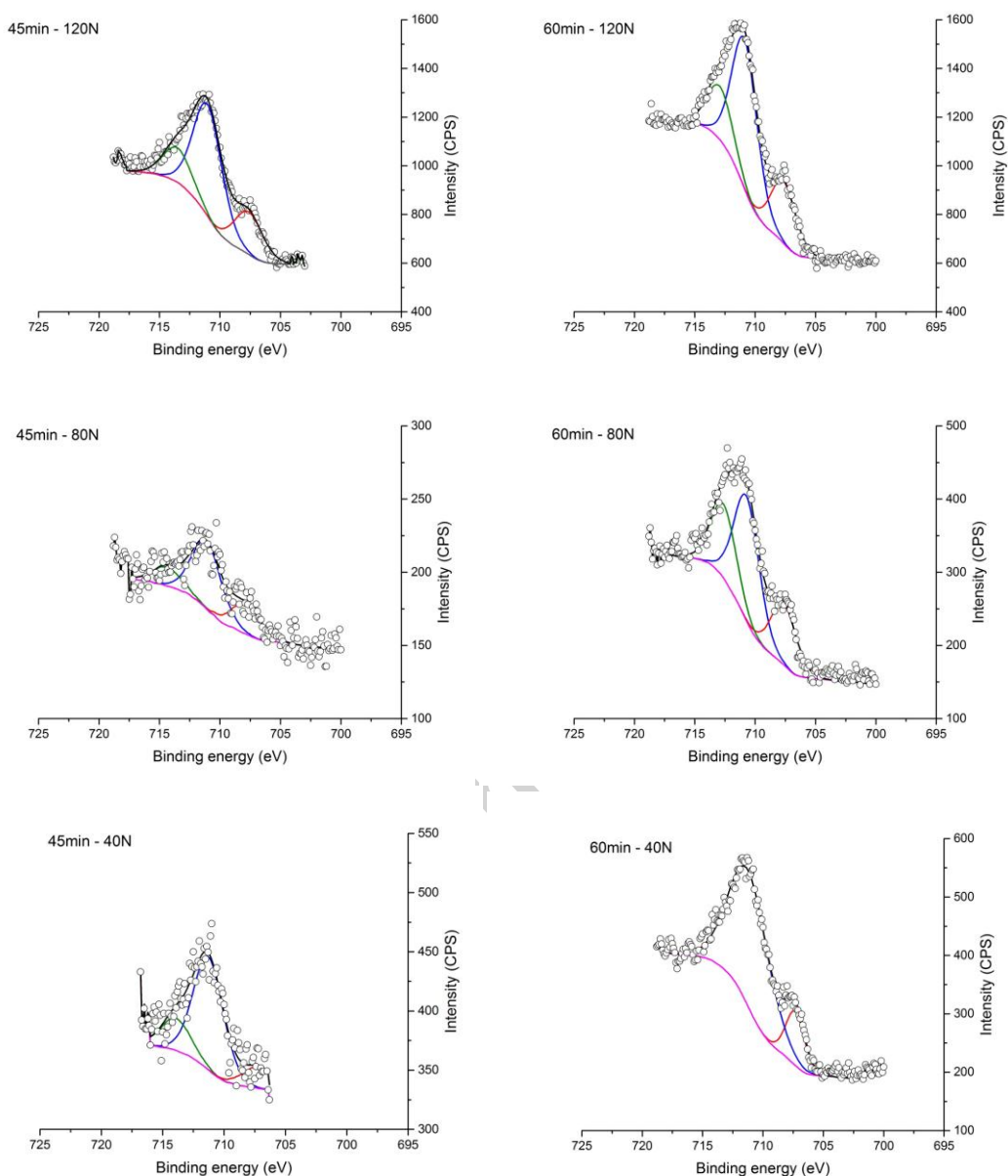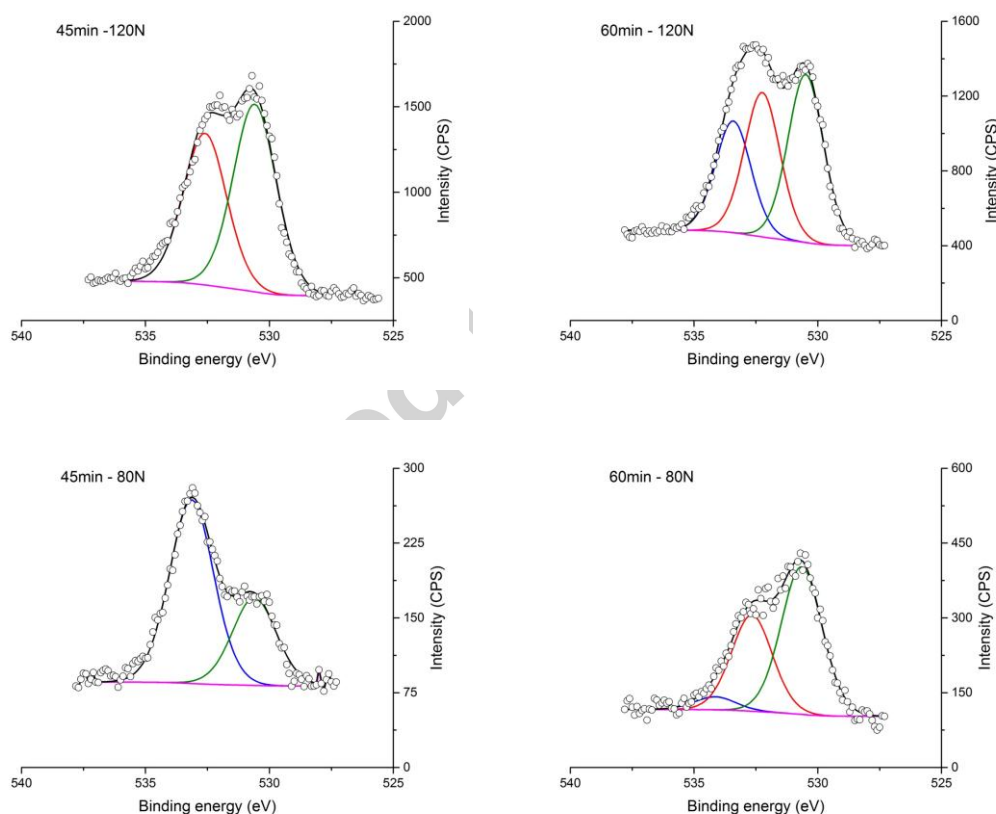

Fig. 3. Fe2p3/2 XPS spectra. Fitting curves belonging to iron (—), iron oxides (—), high binding-energy iron (—) or baseline (—) are also outlined.

As shown in Fig. 4, oxygen appeared as the convolution of three different O1s peaks for tests conducted for 60 minutes, or two peaks for 45 minutes ones. In 60-min case, peaks were found at 533.8 ± 0.4 eV, 532.4 ± 0.3 eV and 530.6 ± 0.1 eV. Taking into consideration the work by Beattie et al. [52], the intermediate binding energy belongs to [NTf$_2$] anion, whereas the lowest binding energy ought to arise from oxides on the surface. Although the surface in their work is gold, Fe$_2$O$_3$ and Au$_2$O$_3$ may have very

close XPS positions around 530.2 eV according to NIST database [50]. The highest binding energy is difficult to identify, but the most probable chemical species is adsorbed water, which has been described to show up at 533.3 eV when adsorbed onto iron surfaces [53]. Sample tested with the highest load showed the highest relative concentration of surface water (~25%) while the ratio of the oxygen bands arising from Fe_2O_3 and $[NTf_2]$ (Fe_2O_3 / $[NTf_2]$ oxygen ratio) is 1.3 ± 0.2 and independent of the load. This value is much higher than the expected 0.75 value for an equimolecular ratio (3 oxygen atoms in a Fe_2O_3 molecule and 4 oxygen atoms in a $[NTf_2]$ molecule). In addition, tests conducted for 45 minutes showed only the peaks from $[NTf_2]$ anion at 532.8 ± 0.3 eV and Fe_2O_3 at 530.7 ± 0.1 eV. It is interesting to state that only the sample tested at 120 N showed a Fe_2O_3 / $[NTf_2]$ oxygen ratio of 1.2, similar to the previous sample. Samples at 80 or 40 N exhibited a lower ratio of 0.5, suggesting the presence of a higher amount of $[NTf_2]$ on the surface.
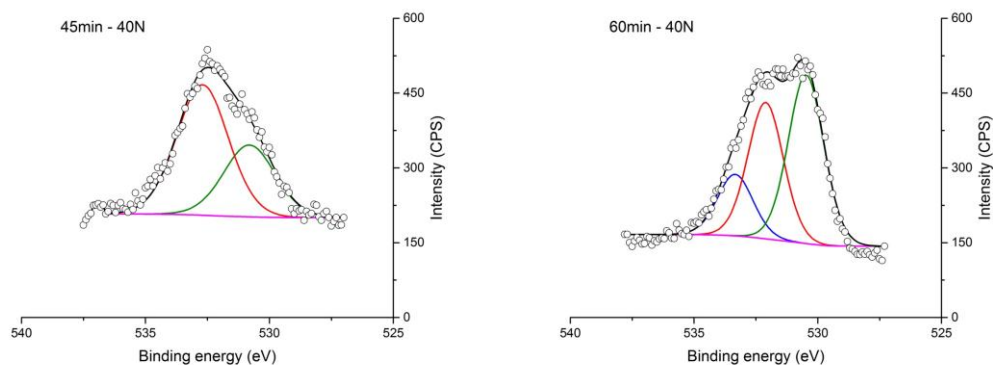
Fig. 4. O1s XPS spectra. Fitting curves assigned to oxides (—), [NTf$_2$] anion (—), adsorbed water (—) or baseline (—) are outlined too.

The presence of ionic liquid or related species on the surface was evaluated following fluorine and nitrogen, which are not present in the composition of the steel (Figs. 5-6).
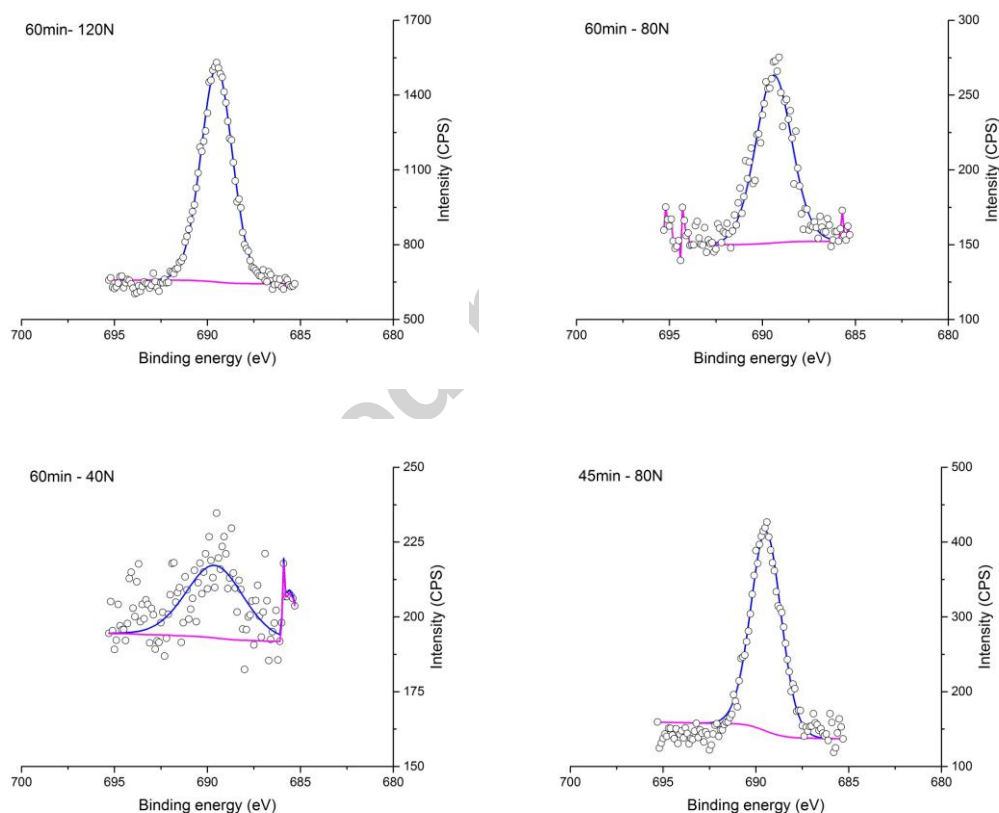

Fig. 5. F1s XPS spectra. Fitting curves assigned to [NTf$_2$] anion (—) or baseline (—) are outlined too.

Samples assayed for 60 minutes showed clear F1s peaks at 689.5 ± 0.1 eV, which fits with the position for C–F bonds in [NTf$_2$] anion [35,53]. However, N1s is clearly seen only in the sample at 120 N, barely observed in the sample at 80 N and negligible in the sample at 40 N. When spotted, N1s appears as a

doublet at 403.4 ± 0.1 eV and 400.3 ± 0.1 eV. Both values correspond respectively to the [NTf$_2$] anion (399.9 eV) and aliphatic ammonium cations (403.2 eV), like [N$_{1888}$] [52]. Taking into consideration the ratio of areas F$_{1s}$ / Fe$_{2p3/2}$ and N$_{1s}$ / Fe$_{2p3/2}$, the amount of N or F is increased with load. This fact points to a lower amount of ionic liquid on the wear scar with lower loads. In the case of 45 minutes samples, only the test carried out at 80 N exhibited a similar behavior, with F1s peak at 689.5 eV and two very noisy N1s peaks at 400.1 and 403.5 eV. Samples tested at 120 and 40 N showed a single N1s peak at 400.5 ± 0.1 eV that does not fit with the signals of [NTf$_2$]. Furthermore, fluorine cannot be detected in either both samples.
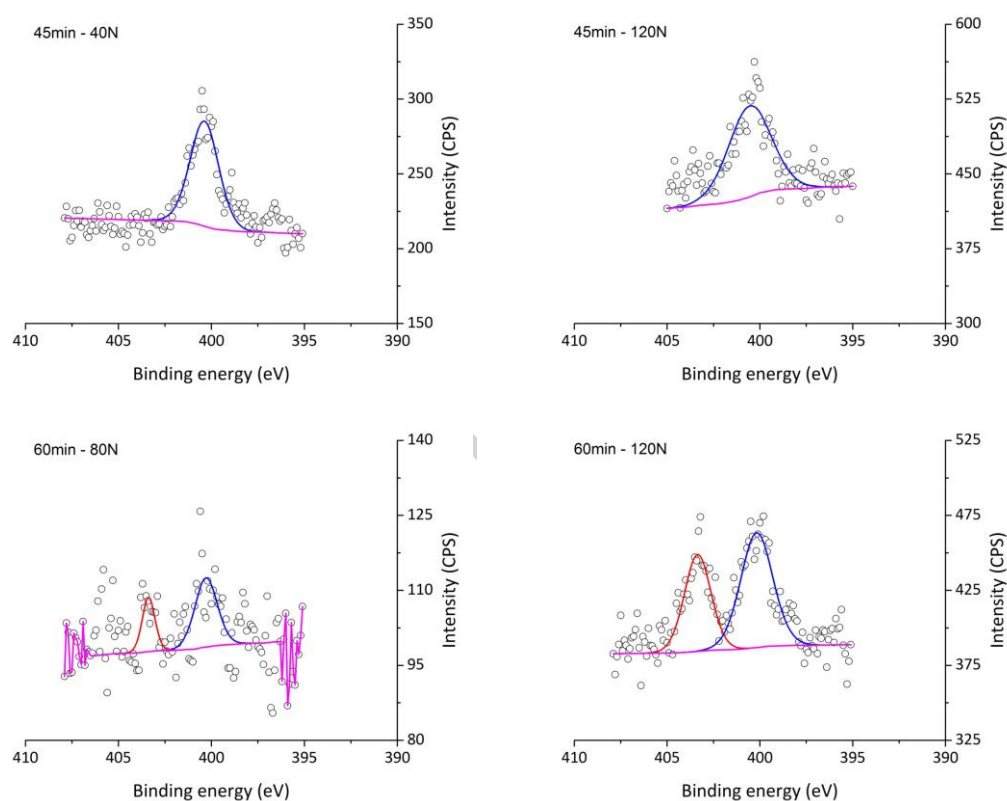

Fig. 6. N1s XPS spectra. Fitting curves assigned to [NTf$_2$] anion (—), aliphatic ammonium cations (—) or baseline (—) are outlined too.

The thickness of the tribolayer was evaluated by following the behavior of iron, nitrogen or fluorine with depth in different tests. In order to do so, samples were sputtered at a 7.2 nm·min^{-1} rate. As shown in Fig. 7, iron composition does not seem to depend greatly on depth with the exception of the sample tested for 45 minutes at 80 N, where the difference in the behavior was more evident. Anyhow, as reflected in Fig. 8, fluorine was followed in samples at 60 minutes whereas nitrogen was followed in samples at 45

minutes. According the obtained results, the ratio of fluorine or nitrogen vs. iron decreased with depth as the tribolayer was being destroyed. In addition, the stabilization of the signal was used as an estimation of the layer thickness (4.8 nm in the sample tested for 60 minutes at 120 N, and 2.4 nm in the samples tested for 60 minutes at 80 N and for 60 minutes at 40 N). In the case of the samples assayed for 45 minutes, the estimated thickness according to nitrogen / iron ratio was 2.4 nm at 120 N and 1.2 nm at 40 N. In the test conducted for 45 minutes at 80 N, both elements were detected in the surface and therefore the tribolayer thickness can be estimated according to either N or F. This estimation results in 3.6 nm when using the F / Fe ratio or 1.2 nm when using the N / Fe ratio), then the mean value of 2.4 nm was used instead. In fact, the content of iron oxides for this sample (Fig. 7) seems to stabilize between 2.4 nm and 3.6 nm as well as the high binding energy iron, which becomes stable around 2.4 nm. According to this, a final thickness of 2.4 nm was assigned for this sample.
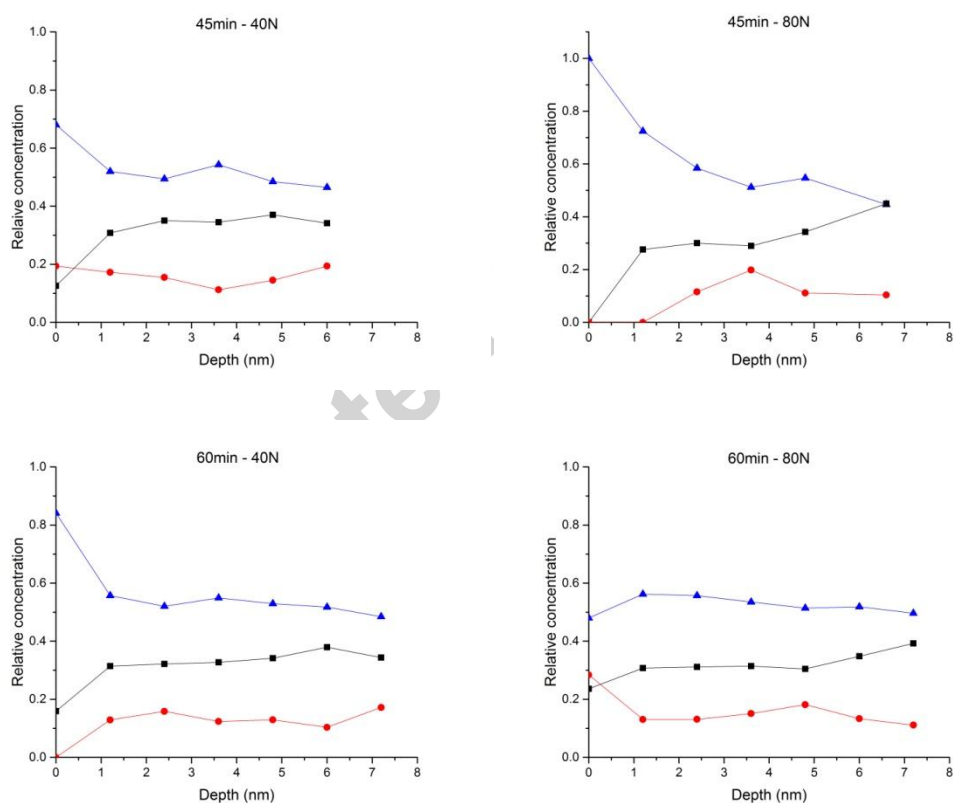

Fig. 7. Behavior with depth of the different species of iron: Fe_2O_3 (▲), metallic iron (■) or high binding-energy iron (●).
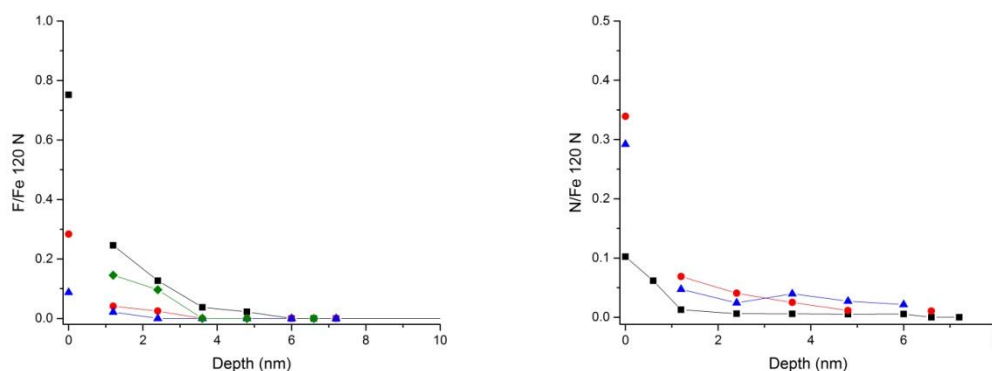
Fig. 8. Behavior with depth of the fluorine (60 minutes) or nitrogen (45 minutes) in different samples: F1s or N1s-40N (▲), F1s or N1s-80N (●), F1s or N1s-120N (■), F1s-40N-45min (◆).

Fig. 9 summarizes the thickness of the different samples, showing a clear trend of thicker layers with higher loads or longer test durations.
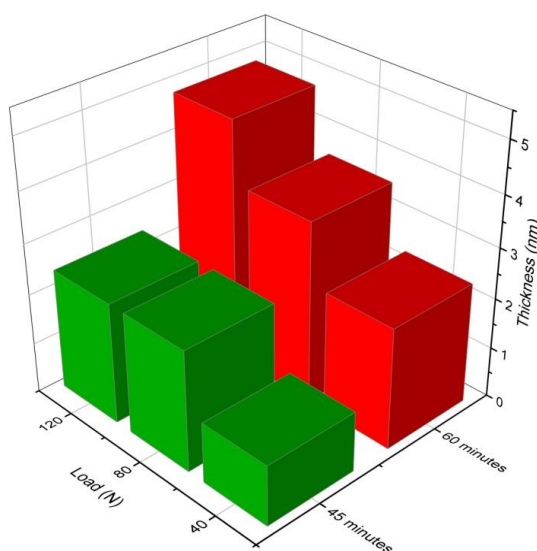

Fig. 9. Estimation of tribolayer thickness according to XPS depth-profiling results.

3.2. Tribological tests at constant load (80 N).

Fig. 10 displayed the evolution of the friction coefficient with the sliding distance in tests carried out varying frequency (10, 15, 20, 25 and 30 Hz) and keeping constant both load (80 N) and sliding distance (432 m) in each case. All tests presented a stable friction behavior with increasing values as frequency decreased due to a lower speed and thinner film thickness. This trend was also found with phosphonate ionic liquids in steel/aluminum contact [54].
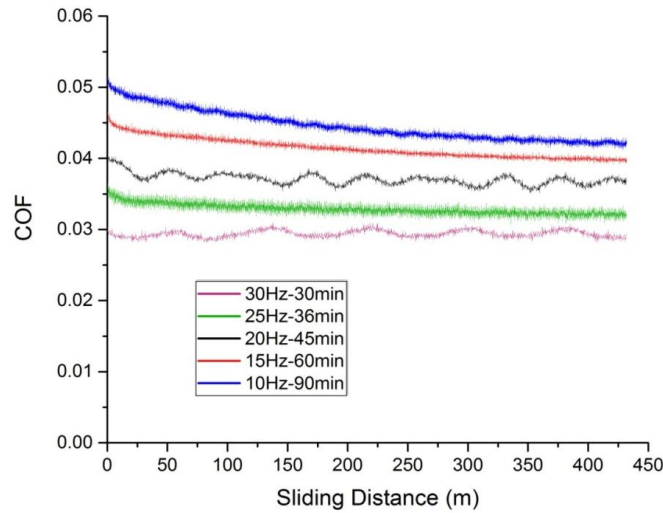
Fig. 10. Evolution of friction coefficient versus sliding distance for tests made at 80 N-load.

Both the average friction coefficient and wear volume for all tests are shown in Fig. 11. The standard deviation of the results did not reach 10% in any case. Although the friction coefficient linearly increased with frequency decrease, the wear volume had a different behavior with decreasing values as frequency diminished from 30 to 20 Hz, and then from 20 to 10 Hz the wear volume started to rise.

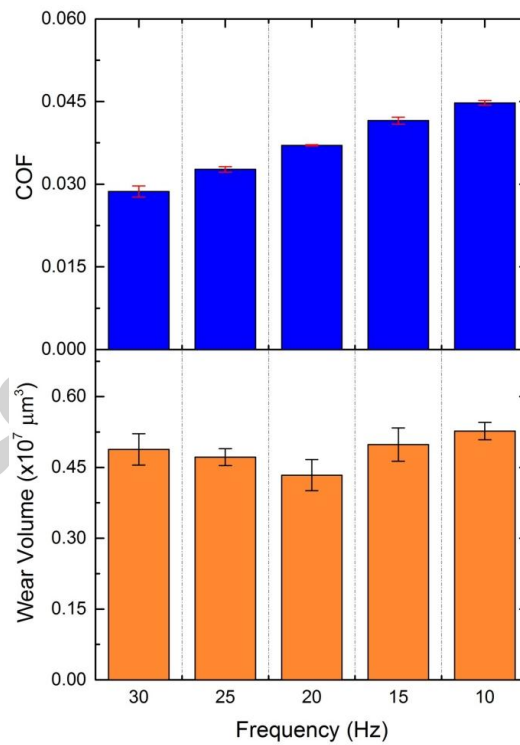Fig. 11. Tribological results from tests made at 80 N-load and sliding distance of 432 m.

Fig. 12 shows SEM images of the wear scar obtained in the variable frequency tests (testing time of 30, 36, 45, 60 and 90 minutes). Unlike what was observed in tests at constant frequency, the SEM images show similar wear track width for all samples. In this case, plastic deformation was also found on the

edge of the wear scar for all samples and the EDS analysis also found only the elements present in the disk material (steel) as it was discussed in section 3.1.

30 min	**36 min**	**45 min**

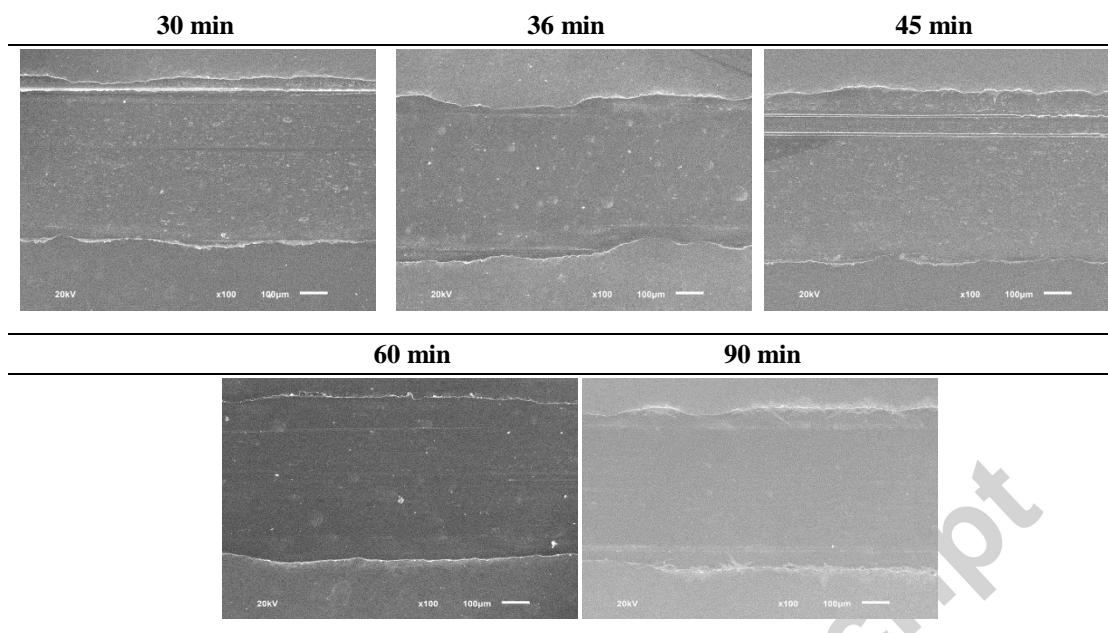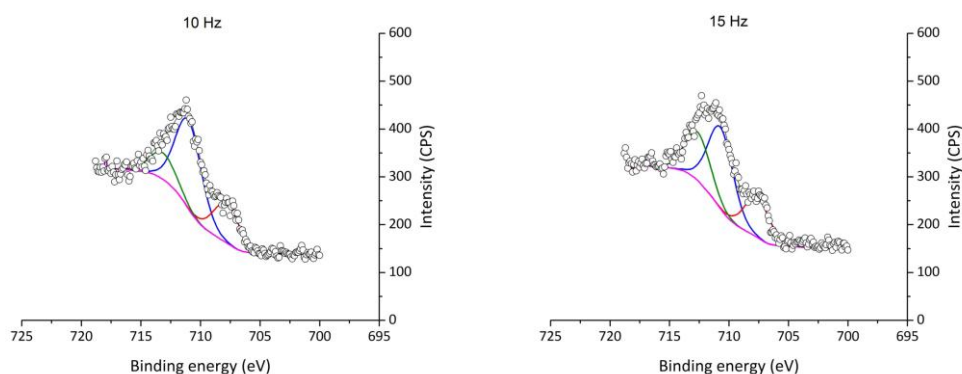| **60 min**	**90 min**

Fig. 12. SEM images (magnification: x100, scale length: 100 μm) from the wear surface after tribological tests made at 80 N-load.

In general, all the samples observed showed similar worn surfaces but a minimum wear value was obtained in the 20 Hz-test. From XPS analysis, the Fe2p3/2 (Fig. 13) can be deconvolved into three peaks at 707.8 ± 0.1 eV, 710.8 ± 0.1 eV and 713.0 ± 0.3 eV, whose nature has been previously discussed. Additionally, the relative intensities of these deconvolved peaks are very similar and around $25 \pm 1\%$ for 707.8 eV, 55 ± 4 % for 710.8 eV and 20 ± 5 % for 713.0 eV.
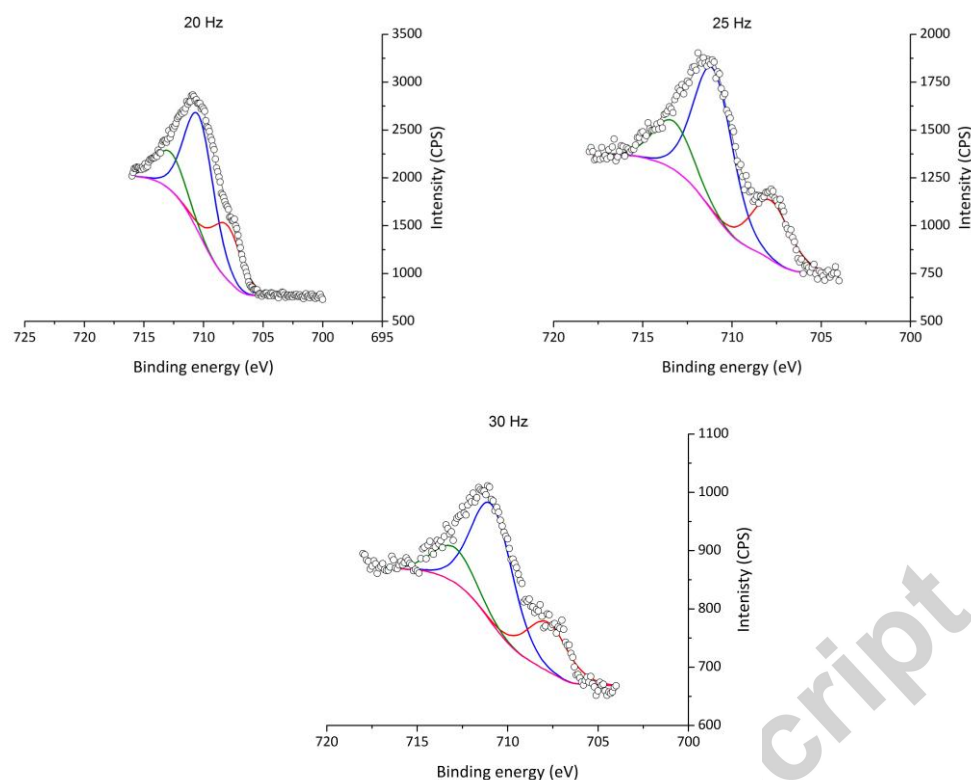
Fig. 13. Fe2p3/2 band for different frequencies. Fitting curves belonging to iron (—), iron oxides (—), high binding-energy iron (—) or baseline (—) are outlined as well.

Regarding the oxygen (Table 3), it appears once again as the combination of three different O1s peaks at 533.8 ± 0.3, 532.7 ± 0.2 and 530.7 ± 0.1 eV expected to be adsorbed water, [NTf$_2$] and iron oxides, respectively. The most interesting issue with the oxygen is the correlation of adsorbed water and iron oxides with the wear volume. The percentage of total oxygen belonging to adsorbed water decreases with the wear volume becoming negligible with the better wear performance sample (20 Hz – 45 minutes). This behavior seems to agree with the previously reported corrosion effect on surface by adding water to ionic liquids [55]. On the other hand, iron oxides showed the opposite trend: the highest percentage value was obtained in the mentioned above test conducted at 20 Hz and 45 minutes.
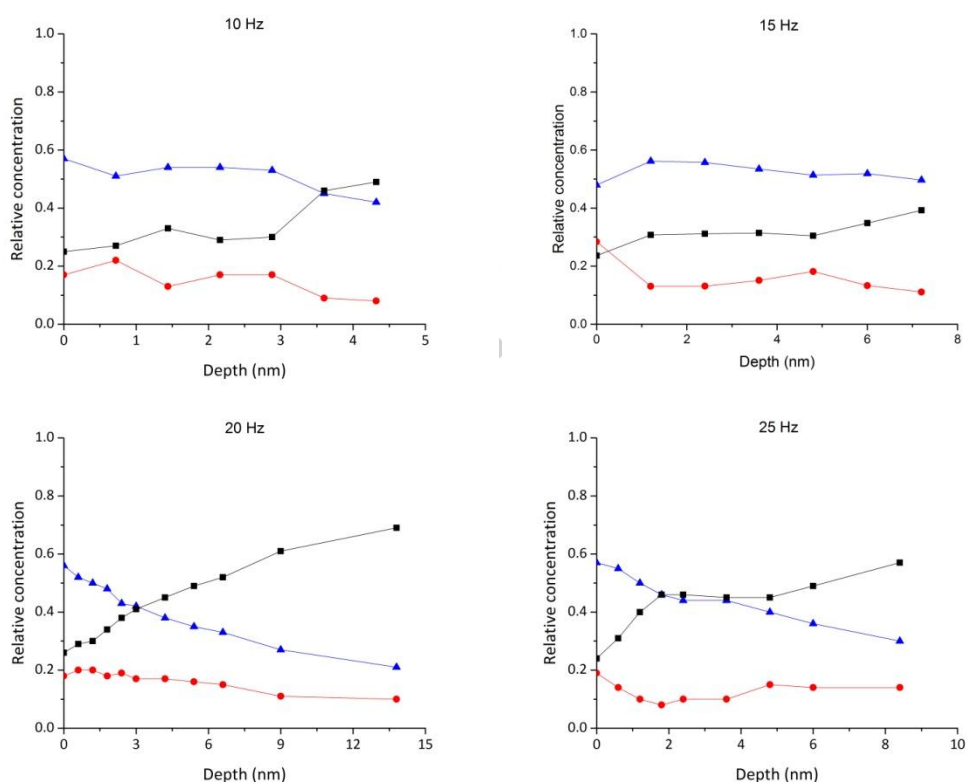
Table 3. Percentage of total oxygen ascribed to water, [NTf$_2$] or Fe$_2$O$_3$ for constant load tests.

Sample	O1s 533.8 - water	O1s 532.7 - [NTf$_2$]	O1s 530.7 - Fe$_2$O$_3$
10 Hz – 90 min	10%	39%	52%
15 Hz – 60 min	5%	37%	57%
20 Hz – 45 min	---	27%	73%
25 Hz – 36 min	13%	37%	50%
30 Hz – 30 min	47%	23%	30%

Now, the Fe_2O_3 / [NTf$_2$] oxygen ratio is independent of the frequency-time combination and its 1.4 ± 0.1 value is much higher than the equimolecular ratio (0.75) previously mentioned in the section 3.1. On the contrary, the 20 Hz – 45 min sample showed a Fe_2O_3 / [NTf$_2$] oxygen ratio of 2.7, suggesting a very little amount of ionic liquid on the surface. F1s could be detected in every sample at 689.6 ± 0.1 eV, belonging to fluorine in [NTf$_2$] anion. However, sample tested at 20 Hz and 45 minutes showed an F1s doublet in the surface layer as previously introduced: a first peak at 689.5 eV related to [NTf$_2$] and a second one at 685.3 eV which is probably due to iron fluorides [35].

Figure 14 shows the relative concentration of iron species with depth profiling an, an evident decreasing trend in the content of iron oxides for samples at 20 and 25 Hz appeared, although it was more remarkable in the first case. The rest of the samples seemed to behave similar, keeping the iron oxides relative concentration mainly constant with depth.
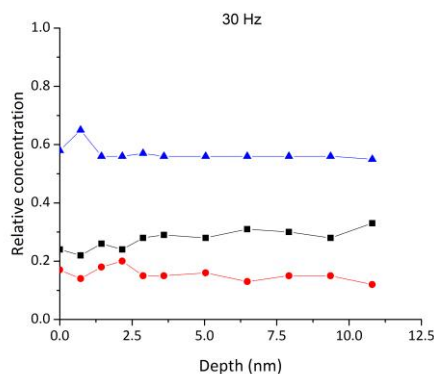
Fig. 14. Fe2p3/2 behaviour with depth for samples with different frequencies and times of the different species of iron: Fe_2O_3 (▲), metallic iron (■), high binding-energy iron (●).

Concerning depth profiling, the test conducted at 20 Hz and 45 minutes displayed a rapid decrease in the F1s associated to $[NTf_2]$ anion and a slower decrease in the F1s associated to metal fluorides. Similarly, in the test at 25 Hz and 36 minutes, Fig. 15, the F1s band of $[NTf_2]$ anion (689.5 eV) is substituted by an F1s band from metal fluoride (685.0 eV) as the depth grows.

Fig. 15. F1s spectra for sample tested at 25 Hz and 36 minutes at different depths: 0 nm (●), 0.6 nm (▲), 1.2 nm (■) and 1.8 nm (◆).

In fact, after 1.8 nm the F1s band from $[NTf_2]$ has completely disappeared whereas the metal fluoride F1s band is evident at deeper layers. Sample assayed at 30 Hz – 30 min behaved similarly. Thus, after 6.5 nm sputtering the single F1s peak of $[NTf_2]$ splitted into two peaks at 685.3 eV (metal fluorides) and 689.0 eV ($[NTf_2]$). Nevertheless, the ratio of areas F1s / Fe2p3/2 clearly decreases with depth in every conducted test, as recorded in Fig. 16.

Fig. 16. Behaviour of F1s / Fe2p3/2 ratio with depth at variable frequency:
10 Hz (●), 15 Hz (▲), 20 Hz (■), 25 Hz (◆) and 30 Hz (★)

This evidence, together with the behavior of iron vs. depth, can be used to estimate the thickness of the tribolayer, recorded in 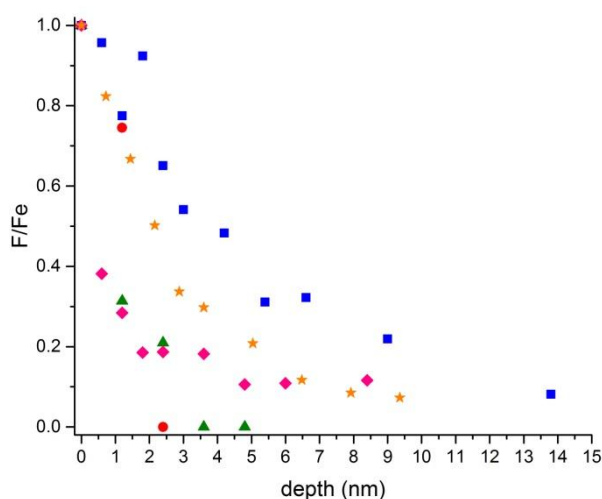Table 4. The wear results obtained are in correspondence with the tribofilm thickness found. The lowest wear result at 20 Hz and 45 minutes are related to the thicker tribofilm formed.

Table 4. Tribolayer thickness of tests conducted at variable frequencies.

Sample	Thickness (nm)
10 Hz – 90 min	2.4
15 Hz – 60 min	3.6
20 Hz – 45 min	14.4
25 Hz – 36 min	1.2
30 Hz – 30 min	6

4. Conclusions

The tribological behavior of a novel [NTf$_2$] anion-based ionic liquid was studied as neat lubricant in a steel-steel contact using a reciprocating ball-on-disk machine under different test conditions. From the results obtained, the following conclusions can be drawn:

- Friction coefficient showed quite similar values in tests made at constant frequency and different load and testing time (or sliding distance). Only one exception was found in test made at both lowest load and testing time because of the dependence of the tribofilm formation process on both testing parameters. On the other hand, wear volume increased with high load as expected.

The increase of wear volume with the sliding distance was only verified under the highest load (120 N) test.

- The worn surface analyses for tests at constant frequency (variable load and sliding distance) exhibited a predominant plastic deformation as wear mechanism. In addition, the best anti-wear behavior is close related to higher values of iron oxide / metallic iron ratio in the wear scar. The growth of tribofilm thickness with increasing load and testing time was also probed.

- In tests made at constant both load and sliding distance, friction values increased with the decrease of frequency, according to typical mixed or boundary lubrication regime. The 20 Hz-tests showed the lowest wear volume, which is related to the thicker tribofilm formed.

- The wear mechanism observed in all cases was dominated by plastic deformation and the XPS analyses showed the chemical interaction of the ionic liquids with surface and determined the tribofilm thickness and its dependency with load, testing time and frequency.

References

[1] Cai M, Guo R, Zhou F, Liu W. Lubricating a bright future: Lubrication contribution to energy saving and low carbon emission. Sci China Technol Sci 2013;56:2888–913. doi:10.1007/s11431-013-5403-2.

[2] Reeves CJ, Menezes PL. Advances in Eco-friendly lubricants for tribological applications: past, present, and future. In: Ecotribology, Materials Forming, Machining and Tribology. J.P. Davim (ed). Springer, 2016.

[3] Ryk G, Etsion I. Testing piston rings with partial laser surface texturing for friction reduction. Wear 2006; 261:792–796. doi:10.1016/j.wear.2006.01.031.

[4]   Ye C, Liu W, Chen Y, Yu L. Room-temperature ionic liquids: a novel versatile lubricant. Chem Commun (Camb) 2001:2244–5. doi:10.1039/B106935G.

[5]   Petkovic M, Seddon KR, Rebelo LPN, Pereira CS. Ionic liquids: a pathway to environmental acceptability. Chem Soc Rev 2011;40:1383–403. doi:10.1039/c004968a.

[6]   Rensselar J Van. Unleashing the potential of ionic liquids. Tribol Lubr Technol 2010;April.

[7]   Smith PG. High-temperature molten-salt lubricated hydrodynamic. J Bear ASLE Trans 1961; 4:263-274.

[8]   Bermúdez MD, Jiménez AE, Sanes J, Carrión FJ. Ionic liquids as advanced lubricant fluids. Molecules 2009;14:2888–908. doi:10.3390/molecules14082888.

[9]   Palacio M, Bhushan B. A review of ionic liquids for green molecular lubrication in nanotechnology. Tribol Lett 2010;40:247–68. doi:10.1007/s11249-010-9671-8.

[10]   Minami I. Ionic liquids in tribology. Molecules 2009;14:2286–305. doi:10.3390/molecules14062286.

[11]   Somers A, Howlett P, MacFarlane D, Forsyth M. A Review of Ionic Liquid Lubricants. Lubricants 2013;1:3–21. doi:10.3390/lubricants1010003.

[12]   Somers AE, Biddulph SM, Howlett PC, Sun J, MacFarlane DR, Forsyth M. A comparison of phosphorus and fluorine containing IL lubricants for steel on aluminium. Phys Chem Chem Phys 2012;14:8224. doi:10.1039/c2cp40736a.

[13]   Qu J, Blau PJ, Dai S, Luo H, Meyer HM. Ionic Liquids as Novel Lubricants and Additives for Diesel Engine Applications. Tribol Lett 2009;35:181–9. doi:10.1007/s11249-009-9447-1.

[14]   Totolin V, Minami I, Gabler C, Dörr N. Halogen-free borate ionic liquids as novel lubricants for tribological applications. Tribol Int 2013;67:191–8. doi:10.1016/j.triboint.2013.08.002.

[15]   Zhang L, Feng D, Xu B. Tribological characteristics of alkylimidazolium diethyl phosphates ionic liquids as lubricants for steel-steel contact. Tribol Lett 2009;34:95–101. doi:10.1007/s11249-009-9412-z.

[16]   Jiang D, Hu L, Feng D. Crown-type ionic liquids as lubricants for steel-on-steel system. Tribol Lett 2011;41:417–24. doi:10.1007/s11249-010-9726-x.

[17]   Mahrova M, Pagano F, Pejakovic V, Valea A, Kalin M, Igartua A, Tojo E. Pyridinium based dicationic ionic liquids as base lubricants or lubricant additives. Tribol Int 2015;82:245–54. doi:10.1016/j.triboint.2014.10.018.

[18] Otero I, López ER, Reichelt M, Fernández J. Friction and anti-wear properties of two tris(pentafluoroethyl) trifluorophosphate ionic liquids as neat lubricants. Tribol Int 2014;70:104–11. doi:10.1016/j.triboint.2013.10.002.

[19] Qu J, Truhan JJ, Dai S, Luo H, Blau PJ. Ionic liquids with ammonium cations as lubricants or additives. Tribol Lett 2006;22:207–14. doi:10.1007/s11249-006-9081-0.

[20] Jiménez AE, Bermúdez MD, Iglesias P, Carrión FJ, Martínez-Nicolás G. 1-N-alkyl -3-methylimidazolium ionic liquids as neat lubricants and lubricant additives in steel-aluminium contacts. Wear 2006;260:766–82. doi:10.1016/j.wear.2005.04.016.

[21] Battez AH, González R, Viesca JL, Blanco D, Asedegbega E, Osorio A. Tribological behaviour of two imidazolium ionic liquids as lubricant additives for steel/steel contacts. Wear 2009;266:1224–8. doi:10.1016/j.wear.2009.03.043.

[22] Mu Z, Zhou F, Zhang S, Liang Y, Liu W. Effect of the functional groups in ionic liquid molecules on the friction and wear behavior of aluminum alloy in lubricated aluminum-on-steel contact. Tribol Int 2005;38:725–31. doi:10.1016/j.triboint.2004.10.003.

[23] Jiménez AE, Bermúdez MD. Imidazolium ionic liquids as additives of the synthetic ester propylene glycol dioleate in aluminium-steel lubrication. Wear 2008;265:787–98. doi:10.1016/j.wear.2008.01.009.

[24] Liu W, Ye C, Gong Q, Wang H, Wang P. Tribological performance of room-temperature ionic liquids as lubricant. Tribol Lett 2002;13:81–5. doi:10.1023/A:1020148514877.

[25] Phillips BS, Zabinski JS. Ionic liquid lubrication effects on ceramics in a water environment. Tribol Lett 2004;17:533–41. doi:10.1023/B:TRIL.0000044501.64351.68.

[26] Wang H, Lu Q, Ye C, Liu W, Cui Z. Friction and wear behaviors of ionic liquid of alkylimidazolium hexafluorophosphates as lubricants for steel/steel contact. Wear 2004;256:44–8. doi:10.1016/S0043-1648(03)00255-2.

[27] Freire MG, Neves CMSS, Marrucho IM, Coutinho JAP, Fernandes AM. Hydrolysis of Tetrafluoroborate and Hexafluorophosphate Counter Ions in Imidazolium-Based Ionic Liquids. J Phys Chem A 2009;114:3744–9. doi:10.1021/jp903292n.

[28] Viesca J-L, Anand M, Blanco D, Fernández-González A, García A, Hadfield M. Tribological Behaviour of PVD Coatings Lubricated with a FAP− Anion-Based Ionic Liquid Used as an Additive. Lubricants 2016;4:8. doi:10.3390/lubricants4010008.

[29] Viesca JL, García A, Hernández Battez A, González R, Monge R, Fernández-González A, Hadfield, M. FAP- anion ionic liquids used in the lubrication of a steel-steel contact. Tribol Lett 2013;52:431–7. doi:10.1007/s11249-013-0226-7.

[30] Hernández Battez A, González R, Viesca JL, Fernández-González A, Hadfield M. Lubrication of PVD coatings with ethyl-dimethyl-2-methoxyethylammonium tris(pentafluoroethyl)trifluorophosphate. Tribol Int 2013;58:71–8. doi:10.1016/j.triboint.2012.10.001.

[31] González R, Hernández Battez A, Blanco D, Viesca JL, Fernández-González A. Lubrication of TiN, CrN and DLC PVD coatings with 1-butyl-1- methylpyrrolidinium tris(pentafluoroethyl)trifluorophosphate. Tribol Lett 2010;40:269–77. doi:10.1007/s11249-010-9674-5.

[32] González R, Battez AH, Viesca JL, Higuera-Garrido A, Fernández-González A. Lubrication of DLC Coatings with Two Tris(pentafluoroethyl)trifluorophosphate Anion-Based Ionic Liquids. Tribol Trans 2013;56:887–95. doi:10.1080/10402004.2013.810319.

[33] Blanco D, González R, Hernández Battez A, Viesca JL, Fernández-Gonzlez A. Use of ethyl-dimethyl-2-methoxyethylammonium tris(pentafluoroethyl) trifluorophosphate as base oil additive in the lubrication of TiN PVD coating. Tribol Int 2011;44:645–50. doi:10.1016/j.triboint.2011.01.004.

[34] Minami I, Kita M, Kubo T, Nanao H, Mori S. The tribological properties of ionic liquids composed of trifluorotris(pentafluoroethyl) phosphate as a hydrophobic anion. Tribol Lett 2008;30:215–23. doi:10.1007/s11249-008-9329-y.

[35] García A, González R, Hernández Battez A, Viesca JL, Monge R, Fernández-González A, Hadfield M. Ionic liquids as a neat lubricant applied to steel-steel contacts. Tribol Int 2014;72:42–50. doi:10.1016/j.triboint.2013.12.007.

[36] Blanco D, Battez AH, Viesca JL, González R, Fernández-González A. Lubrication of CrN coating with ethyl-dimethyl-2-methoxyethylammonium tris(pentafluoroethyl)trifluorophosphate ionic liquid as additive to PAO 6. Tribol Lett 2011;41:295–302. doi:10.1007/s11249-010-9714-1.

[37] Kheireddin BA, Lu W, Chen IC, Akbulut M. Inorganic nanoparticle-based ionic liquid lubricants. Wear 2013;303:185–90. doi:10.1016/j.wear.2013.03.004.

[38] Pisarova L, Gabler C, Dörr N, Pittenauer E, Allmaier G. Thermo-oxidative stability and corrosion properties of ammonium based ionic liquids. Tribol Int 2012;46:73–83. doi:10.1016/j.triboint.2011.03.014.

[39] Cai M, Liang Y, Yao M, Xia Y, Zhou F, Liu W. Imidazolium ionic liquids as antiwear and antioxidant additive in poly(ethylene glycol) for steel/steel contacts. ACS Appl Mater Interfaces 2010;2:870–6. doi:10.1021/am900847j.

[40] Gabler C, Dörr N, Allmaier G. Influence of cationic moieties on the tribolayer constitution shown for bis(trifluoromethylsulfonyl)imide based ionic liquids studied by X-ray photoelectron spectroscopy. Tribol Int 2014;80:90–7. doi:10.1016/j.triboint.2014.06.018.

[41] Monge R, González R, Hernández Battez A, Fernández-González A, Viesca JL, García A, Hadfield M. Ionic liquids as an additive in fully formulated wind turbine gearbox oils. Wear 2015;328-329:50–63. doi:10.1016/j.wear.2015.01.041.

[42] Somers AE, Howlett PC, Sun J, MacFarlane DR, Forsyth M. Transition in wear performance for ionic liquid lubricants under increasing load. Tribol Lett 2010;40:279–84. doi:10.1007/s11249-010-9695-0.

[43] Murakami T, Kaneda K, Nakano M, Korenaga A, Mano H, Sasaki S. Tribological properties of Fe7Mo6-based alloy under two ionic liquid lubrications. Tribol Int 2008;41:1083–9. doi:10.1016/j.triboint.2008.02.017.

[44] Bandeira P, Monteiro J, Baptista AM, Magalhães FD. Tribological performance of PTFE-based coating modified with microencapsulated [HMIM][NTf$_2$] ionic liquid. Tribol Lett 2015;59. doi:10.1007/s11249-015-0545-y.

[45] Somers AE, Khemchandani B, Howlett PC, Sun J, Macfarlane DR, Forsyth M. Ionic liquids as antiwear additives in base oils: Influence of structure on miscibility and antiwear performance for steel on aluminum. ACS Appl Mater Interfaces 2013;5:11544–53. doi:10.1021/am4037614.

[46] Minami I, Inada T, Sasaki R, Nanao H. Tribo-Chemistry of Phosphonium-Derived Ionic Liquids. Tribol Lett 2010;40:225–35. doi:10.1007/s11249-010-9626-0.

[47] Hernández Battez A, Bartolomé M, Blanco D, Viesca JL, Fernández-González A, González R. Phosphonium cation-based ionic liquids as neat lubricants: Physicochemical and tribological performance. Tribol Int 2016;95:118–31. doi:10.1016/j.triboint.2015.11.015.

[48] Qu J, Bansal DG, Yu B, Howe JY, Luo H, Dai S, Li H, Blau PJ, Bunting BG, Mordhukovich G, Smolenski DJ . Antiwear performance and mechanism of an oil-miscible ionic liquid as a lubricant additive. ACS Appl Mater Interfaces 2012;4:997–1002. doi:10.1021/am201646k.

[49] Fro AP, Kremer H, Leipertz A. Density , Refractive Index , Interfacial Tension , and Viscosity of Ionic Liquids [EMIM][EtSO$_4$], [EMIM][NTf$_2$], [EMIM][N(CN)$_2$], and [OMA][NTf$_2$] in Dependence on Temperature at Atmospheric Pressure. J Phys Chem B 2008;112:12420–30.

[50] http://srdata.nist.gov/xps/Default.aspx, last consulted march 2016.

[51] Bovio S, Podesta A, Lenardi C, Milani PJ. Evidence of extended solid-like layering in [Bmim][NTf$_2$] ionic liquid thin films at room-temperature. Chem. Phys. B 2009;113:6600-6603.

[52] Beattie DA, Harmer-Bassell SL, Ho TTM, Krasowska M, Ralston J, Sellaperumage PMF, Wąsik P. Spectroscopic study of ionic liquids adsorption from solution onto gold. Phys. Chem. Chem. Phys. 2015;17:4199-4209; DOI: 10.1039/C4CP05558F.

[53] Grosvenor AP, Kobe BA, McIntyre NS. Studies of the oxidation of iron by water vapour using X-ray photoelectron spectroscopy and QUASES. Surface Science 2004;572:217-227.

[54] Han Y, Qiao D, Zhang L, Feng D. Study of tribological performance and mechanism of phosphonate ionic liquids for steel / aluminum contact. Tribol Int 2015;84:71–80.

[55] Uerdingen M, Treber C, Balser M, Schmitt G, Werner C. Corrosion behaviour of ionic liquids. Green Chem 2005;7:321. doi:10.1039/b419320m.

Highlights

- Friction and wear reduction is related to tribofilm formation and thickness.

- Tribofilm thickness increases with load and testing time.

- At fixed load tribofilm thickness depend on frequency or speed.